

# DETECTING THE ORIGINS OF SOME FAILURES OF MECHATRONIC DEVICES AND SYSTEMS BY NON-CONTACT, FULL-FIELD LASER SPECKLE INTERFEROMETRY

Borza D.N., Nistea I.T.

INSA Rouen – LMR - LOFIMS, B.P. 8, Avenue de l'Université, 76801 Saint-Etienne du Rouvray, France,  
ioana.nistea@insa-rouen.fr

**Abstract.** *Embedded electronics are exposed to harsh working conditions. They are exposed to high levels of stress having both thermal and mechanical external origins, often coupled. These stressing sources may directly create reliability problems, but they may also increase the effects of other factors, such as humidity, chemical or electrical ones. The experimental analysis of such phenomena may be of great help in discovering the origins of similar failures and in developing a correct numerical model which allows further simulations and establishing credible failure scenarios. The objective of this paper is to present the practical application of a full-field, non-contact optical technique – the out-of-plane speckle interferometry – in finding the physical origins of some failures occurring in an assembled embedded board. The failures appear as solder joint shear in presence of thermo-mechanical stressing. The authors applied a multi-level experimental methodology allowing to obtain the out-of-plane deformation cartography and finally explain the possible root origins of the failures. The test methodology is able to provide an insight into the physics-of-failure. The interferometric sensitivity allows using very small thermal stress, so that they are not inducing any harm to the tested product. The results may further be compared to those of a numerical model.*

**Keywords:** *thermo-mechanical stressing, embedded electronics, speckle interferometry, physics-of-failure.*

## 1. INTRODUCTION

Embedded, surface mount technology electronic board assemblies are multi-material, multi-body, electrically active mechatronic structures. They are characterized by a great variety of physical, as well mechanical as thermal properties.

Their thermo-mechanical properties are determined by the characteristics of the different materials, which may have differences of several orders of magnitude. They are also determined by their macroscopic geometrical parameters (component dimensions and placement) and boundary conditions (type of mounting, casing of the board). In order to develop reliable finite element models, a correct estimation of these factors is necessary.

Experimental evaluation of the surface strain induced by thermal stress in sensitive areas like solder joints becomes thus an important stage in the conception and optimization of embedded electronic systems [1], [9].

The mechanical strain measurement technique must have an adequate sensitivity and must not contribute to the mechanical loading of the tested structures. Pointwise and full-field optical techniques and measurement methods are thus often representing the best choice.

Most widely used experimental full-field optical techniques are digital image correlation, moiré interferometry, in-plane speckle interferometry, shadow moiré, projection moiré, laser Doppler vibrometry. These techniques are characterized by:

- different sensitivities with respect to the displacement to be measured;

- different directions of measurement sensitivity – in-plane, out-of-plane or 3D;

- different sensitivities with respect to physical quantities and phenomena influencing the measurement: temperature, vibrations, humidity, ambient light;

- different levels of complexity of the equipments being used;

- their dynamic properties and real-time capabilities.

Digital image correlation [12] is a low and medium sensitivity technique for measuring static and dynamic displacements. It is characterized by very simple equipments, mainly a lighting source and one or several cameras.

Moiré interferometry [11] makes use of a phase grating attached to the object under test. It interacts with a virtual reference grating and form moiré fringes related to the in-plane displacement fields. The sensitivity is high, about a half of the wavelength for each fringe.

Scanning electronic microscopy [12] allows obtaining very large depth of field micrographs able to achieve very high magnifications. Nanoscale objects may thus be measured. The equipment used is very costly.

In shadow moiré [11], the moiré pattern is produced by the superposition of two regularly spaced gratings which interfere geometrically. Like projection moiré [8], it may be used to measure out-of-plane displacements (like warpage, for example) and 3D shapes with low and medium sensitivity.

Speckle interferometry with in-plane sensitivity [7] has interferometric sensitivity and uses laser light.

## 2. PRINCIPLES OF SPECKLE INTERFEROMETRY

Speckle interferometry (SI) is a well established full field interferometric technique which allows real time and non-contact displacement measurements, yielding accurate and high resolution results [9], [10].

The measurement principle is based on the properties of coherent light which enable the apparition of the phenomenon of interference. Interference makes appear in an optical field random speckles depending upon the phases of interfering waves. Since the phase of a wave depends upon the optical path, this is about the position of the scattering points on the surface of an object, 2D static or dynamic displacement information in the form of fringe patterns may be recorded, superimposed on the image of the tested object [6].

There are many implementations of the technique that vary in terms of type of illumination (continuous, stroboscopic, pulsed), measured quantities (deformation, deformation slopes, form, vibration amplitudes), system geometry, number of interfering waves, or data processing.

The work presented in this paper relies on the use of a continuous wave SI system.

### 2.1 Out of plane speckle interferometry

The basic setup is shown in Figure 1. The most important components of the measurement system are the 100 mW frequency-doubled Nd-YAG laser, a CCD camera and a dedicated 16-bit pipelined processor. The system also provides some additional components for interferometric movie recording.

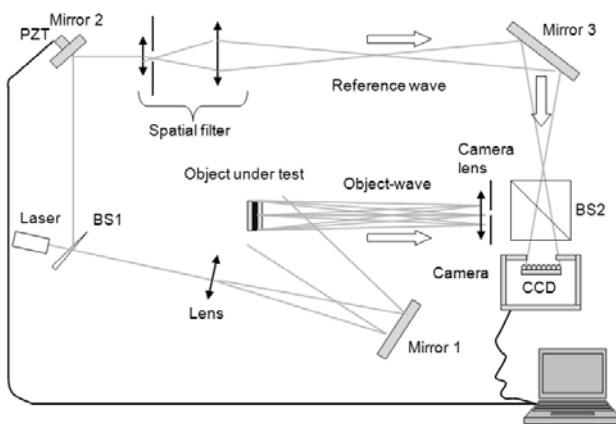


Figure 1. Out of plane speckle interferometry setup

The beam emitted by the laser source is separated by the beam splitter (BS1) into a measuring and a reference beam that travel on separate paths in the interferometer. The wavefront reflected from the tested surface is focused into the CCD plane, where it interferes with the reference wave. The camera lens is translated in order to allow inserting a beam splitter (BS2) so as to obtain a zero angle tilt between the two interfering wavefronts.

This is necessary in order to allow the camera to read the interference fringes.

The instantaneous intensity of the interference field at any pixel (x,y) of the CCD grid can be described by:

$$i_{(x,y)} = I_B + I_M \cdot \cos \varphi(x, y) \quad (1)$$

where  $I_B, I_M$  are the background and the modulation intensities, while  $\varphi(x, y)$  is the relative optical phase between the two wave fronts containing the information on the surface deformation.

Equation 1 has three unknown variables - in order to find the solution, we introduce a known variation in the optical path of the reference beam [8]. The relative optical phase will thus be given by:

$$\varphi = \varphi_{sp} + \Delta\varphi_{obj} + \Delta\varphi_{ref} \quad (2)$$

where:

- $\varphi_{sp}$  is the random phase component introduced by the speckle phenomenon;
- $\Delta\varphi_{obj}$  describes the displacement field of the test surface and
- $\Delta\varphi_{ref}$  is the known phase variation introduced into the reference wave.

The phase-stepping algorithm is implemented by means of a piezoelectric actuator (PZT) attached to a mirror and placed in the reference arm of the interferometer.

For a standard four bucket phase-stepping algorithm, we have:

$$\Delta\varphi_{ref} = \frac{\pi}{2}(k-1), \quad k = 1 \dots 4 \quad (3)$$

We obtain series of 4 primary data fields, described by:

$$\begin{aligned} I_1 &= I_B + I_M \cdot \cos \varphi \\ I_2 &= I_B - I_M \cdot \sin \varphi \\ I_3 &= I_B - I_M \cdot \cos \varphi \\ I_4 &= I_B + I_M \cdot \sin \varphi \end{aligned} \quad (4)$$

#### 2.1.1 Static deformations

For a static or quasi-static deformation, the wrapped optical phase distribution is finally obtained by applying:

$$\varphi = \tan^{-1} \frac{I_4 - I_2}{I_1 - I_3} \quad (5)$$

The wrapped optical phase distributions contains the information related to the out of plane component of the thermally imposed static or quasi-static deformation,  $d(x,y)$ :

$$\varphi(x, y) = \frac{4\pi}{\lambda} d(x, y) \quad (6)$$

A more rigorous analysis may show that in fact the phase is the dot product between the displacement vector associated to each object surface point,  $\vec{d}(x, y)$  and a sensitivity vector associated to that point,  $\vec{K}(x, y)$  :

$$\varphi(x, y) = \frac{4\pi}{\lambda} \vec{d}(x, y) \cdot \vec{K}(x, y) \quad (7)$$

In out-of-plane speckle interferometry the direction of the sensitivity vector is close to the observation direction.

The wrapped phase maps are processed and displayed in real time on the system monitor. An example is shown in the upper part of Figure 2, representing the out-of-plane displacement field of the bare PCB of a tested embedded assembly, fixed in the four corners. These parametric images need to be processed by appropriate algorithms in order to obtain a quantitative estimation of the displacement. The wrapped out-of plane thermal deformation field is obtained by subtracting the phase maps corresponding to the reference and loaded states, and then the optical phase maps are calculated by applying a phase unwrapping procedure. The result may be presented as a 3D surface, as in the lower part of Figure 2.

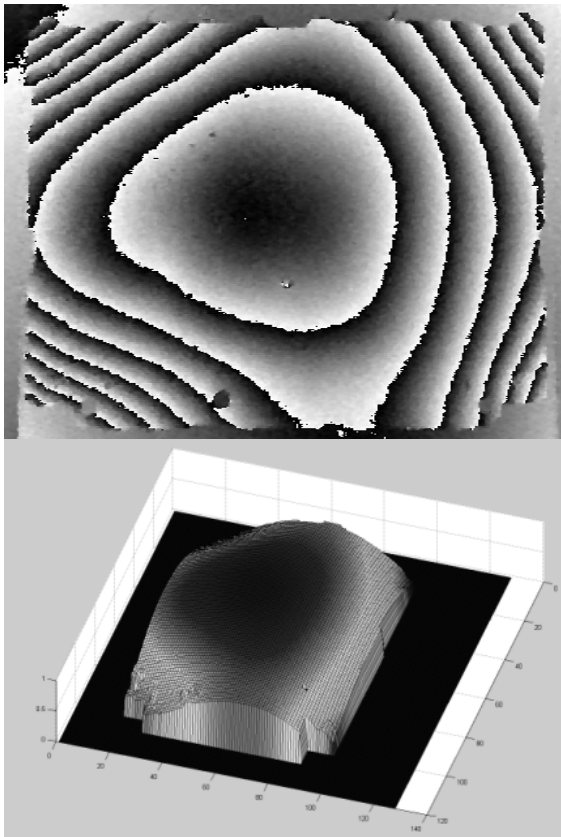


Figure 2. Wrapped (upper part) and unwrapped (lower part) full displacement map of the bare PCB fixed in the 4 corners

The deformation field in Figure 2 represents the side of the PCB opposite to the side where the components are to be placed.

The lack of symmetry in the fringe pattern is due to the lack of symmetry of the different copper layers inside and at the surface of the PCB. The fringe pattern may also be influenced by the asymmetrical boundary conditions and the casing deformation.

### 2.1.2 Vibrations: time-average speckle interferometry

The technique may also be used to study, by the time-average method, the vibration modes and eigenvalues of the tested structure. In these cases, the acquisition rate of the camera (typically 25 - 50 fps for standard cameras) is usually much lower than the vibration frequency of the tested surface. Consequently, the recorded intensity of the interference field will represent an average of the intensity over several cycles of vibration over the exposure period:

$$I_{(x,y)} = I_B + I_M \cdot \int_{T_{exp}} \cos \varphi_{(x,y,t)} dt \quad (8)$$

where the relative optical phase is time dependant due to the sinusoidal surface displacement:

$$\varphi = \varphi_{sp} + \Delta\varphi_{ref} + \frac{4\pi}{\lambda} A_{vib} \sin(\omega_{vib}t + \phi) \quad (9)$$

The recorded intensity can be written as:

$$I_{(x,y)} = I_B + I_M \cdot \cos \varphi_0 \cdot J_0\left(\frac{4\pi}{\lambda} A_{vib}\right) \quad (10)$$

where  $J_0(z)$  the Bessel function of zero order and first kind having as argument  $z$ .

By applying a phase stepping algorithm (similar to the one described for the static measurements) we obtain the time averaged hologram intensity used for high-resolution measurement of the full out-of-plane vibration amplitude field:

$$I_{TAV} = \sqrt{(I_1 - I_3)^2 + (I_4 - I_2)^2} \quad (11)$$

The expression of the time-averaged fringe pattern is:

$$I_{TAV} = I_O \cdot J_0^2\left[\frac{4\pi}{\lambda} \cdot d(x, y)\right] \quad (12)$$

In Equation (12),  $I_O$  represents the image of the object. The calculated intensity map consists of the image of the tested surface superimposed with a fringe pattern, as exemplified below.

Figure 3 presents one of the eigenmodes of the bare PCB recorded by the time-average method.

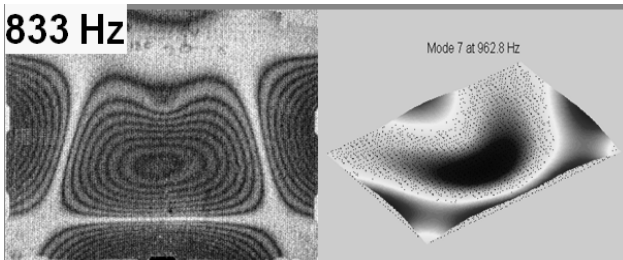


**Figure 3. Eigenmode of the bare PCB. At left, TAV pattern; at right, vibration amplitudes predicted by a numerical model.**

At left, we have the fringe pattern; at right, the explicit vibration amplitude distribution across the surface. The PCB was assembled in its casing by using all five screws.

There isn't a generally accepted numeric procedure for computing the vibration amplitude maps from the Bessel fringe patterns. The methods available for static measurements can't be applied in the case of vibration measurements, as the quantity of interest (optical phase related to the vibration amplitude) is embedded as argument of the Bessel function  $J_0$ .

Noise reduction of the TAV fringes may be achieved by frame averaging and by speckle averaging.

In order to obtain a quantitative estimation for the TAV interferograms, we apply a semi-automated fringe indexing algorithm developed at the Photomechanics laboratory of INSA Rouen. As shown in Figure 4, the algorithm relies on the fact that the values of  $z$  for the zero-crossings of  $J_0(z)$  (corresponding to the dark fringes in the fringe pattern) are well known, therefore, by identifying the order of fringes and subsequently, by applying a local inversion of the Bessel function, one can successfully obtain the unwrapped amplitude maps.

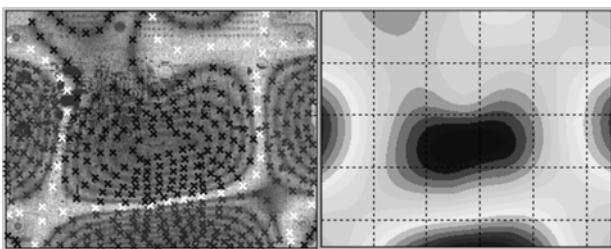


**Figure 4. Fringe indexing procedure on the left and unwrapped amplitude map on the right**

In Equation 9, the trigonometric term represents a high frequency noise that covers the Bessel fringes containing the valuable information.

An alternative method for obtaining the unwrapped phase distributions that allows removing the high frequency noise from the orthogonal components of a high-resolution TAV hologram, is described in [2].

## 2.2 In-plane speckle interferometry

A standard in-plane sensitive measurement setup is presented in Figure 5.

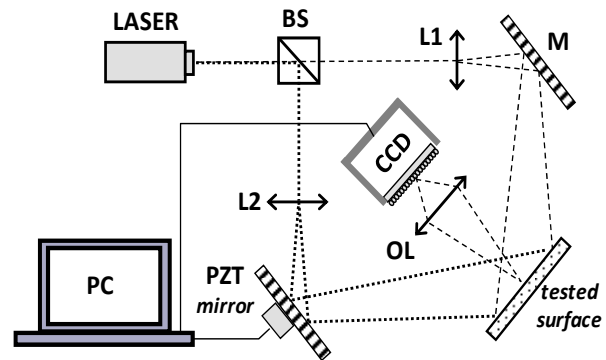


**Figure 5. In plane speckle interferometry setup**

In this case, the interference is created between two measurement waves obtained by dividing the laser emitted beam with beam splitter BS. The illumination directions are symmetrical with respect to the observation direction of the experimental setup so that the sensibility vector is tangent to the tested surface.

The two examples shown in Figure 6 represent the thermal deformation fields of the electronic assembly, following the (horizontal)  $x$  direction (upper image) and respectively the (vertical)  $y$  direction (the lower image).



**Figure 6. In plane thermal deformation fields**

When compared to the thermal deformation fields obtained by the out of plane SI, these results show a higher noise content. This results from both of the interfering waves being speckle waves, as opposed to the out of plane setup, where the reference wave is smooth.

## 3. EXPERIMENTAL SETUP

The experimental setup and results presented from here on concern the out of plane measurements.

### 3.1 Mechanical setup and assembled board

The tested structure (Figure 7) is an electronic board (110 x 150 x 1,8 mm) with a surface mounted PQFP

component of large dimensions (40 x 30 mm), 265 leads 0,5 mm lead pitch. The complete system included the board and its protective housing assembled by 5 fastening screws. Two boards were studied: one without components (the bare PCB) and a completely populated board.

The thermal stress was applied by convection, by using a small heat gun. Speckle interferometry data acquisition may be time- or temperature driven.

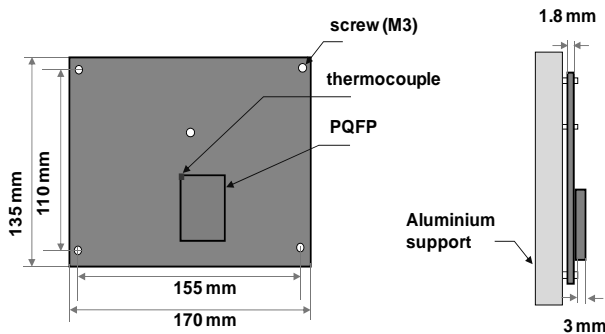


Figure 7. Tested board

The board casing was fixed in a home-made support (Figure 8) so as to be maintained vertical and mechanically stable.

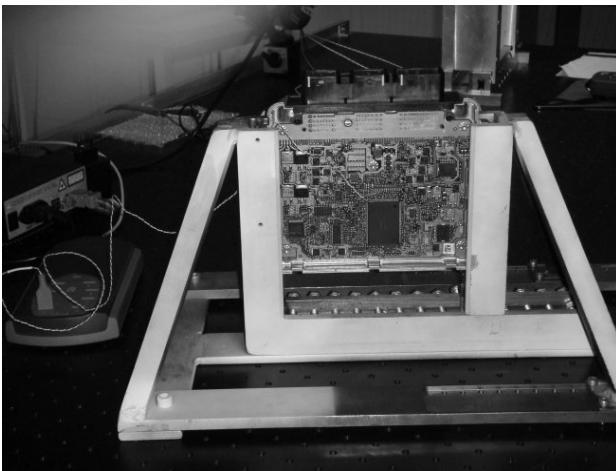


Figure 8. Casing and support

### 3.2 Thermal stressing (quasi-static deformations)

Thermal stress is applied by convection, using a hot air blowing gun. The approximate temperature measurement is done by thermocouples (as seen in Figure 8), for fast heating with 20-35° C, followed by natural cooling. Data logging and provisions for time- or temperature-triggered interferogram data recording is achieved by home-made software (Figure 9).

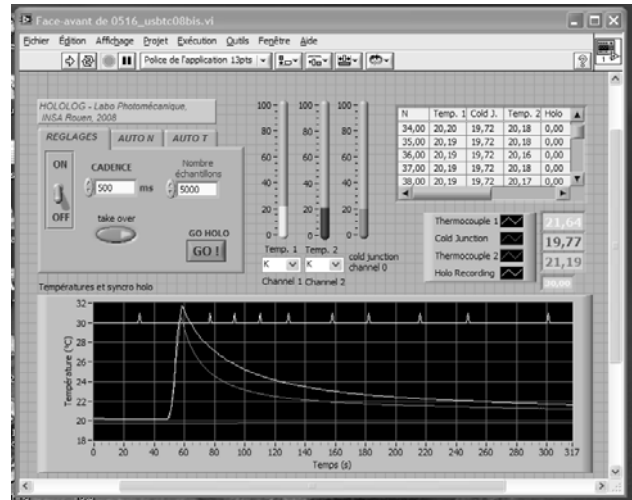


Figure 9. Temperature logging and triggering of interferometric recordings

Heating by convection, by blowing hot air, strongly affects for a few seconds the values of the optical refraction index of air. Interferometric techniques measure the variations of an optical path  $r$ , which is the product between the geometric path  $d$  and the optical refraction index  $n$ ,  $r = d \cdot n$ . If both quantities are varying,  $\Delta r = d \cdot \Delta n + n \cdot \Delta d$ . The measurement of the deformation  $\Delta d$  is temporarily rendered impossible. As soon as the air movement ends,  $\Delta n = 0$  thus the deformation can be measured.

Any two correlograms recorded at the triggering instants seen in Figure 9 may be combined to form an interferogram showing the full-field of deformations occurring between the two instants.

### 3.3 Vibration stressing

We use a pointwise excitation by means of a PZT transducer driven by a frequency generator. We apply a sinusoidal excitation signal, of variable amplitude and frequency. An acoustic excitation, by means of a loudspeaker, can also be applied.

In order to detect the resonance frequencies the excitation frequency is varied over a given interval while the TAV hologram is monitored in real time on the system display. Once the Bessel fringes are detected, the frequency is finely tuned around the resonance peaks (maximum density of fringes).

## 4. EXPERIMENTAL RESULTS

### 4.1 Static deformations by thermal stressing

In a first stage of the experimental examination, the inspection of the assembled board was done at a global level. The purpose was to understand the main differences between the behaviour of the PCBA with respect to the bare PCB and the influence of the macro-mechanical boundary conditions in presence of the thermal stressing. The measurements are done on the

side opposite to the components, so that the fringe pattern represents deformation of the whole PCB, including the regions where the critical components are placed. The conclusions of this preliminary inspection were expected to help in a second, more detailed analysis at a local level, on the side where the components are placed.

**4.1.1 Results at a global level for the 4-point mounted assembly. Thermo-mechanically stressed, fully populated board.**

The interferogram in Figure 10 was recorded in the same configuration as the one presented in Figure 2, with the exception of the fact that the PCB was fully populated. The two fringe patterns are similar; however, the fringe pattern curvatures are different in the upper part of the two fringe patterns, where it's the place of the PQFP component. The interpretation is obvious: the curvature modification of an out-of-plane displacement field is directly related to a flexure moment applied in that region. It may only come from the PQFP component. It means the component is in a stress state.

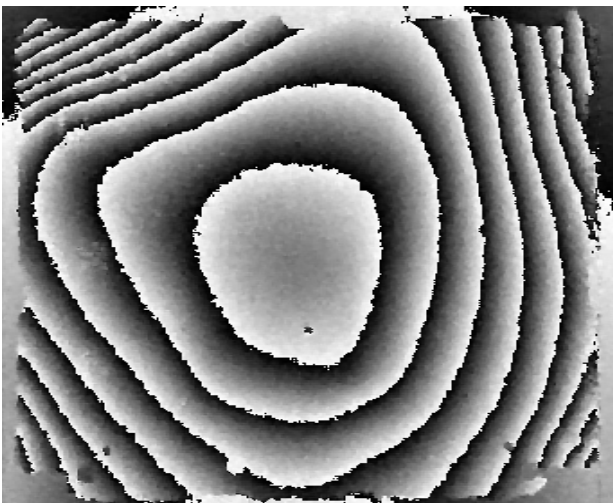


Figure 10. Wrapped full displacement map of the populated board fixed in the 4 corners, seen from the side opposite to the components

Finally, Figure 11 presents the fringe pattern for the fully populated PCB assembled by 4 screws, but seen from the components side. The large component is in the lower part of the image. It may be identified by the rather rectilinear fringe pattern across it. It means that the component remains almost plane, while the PCB around is in out-of-plane flexure.

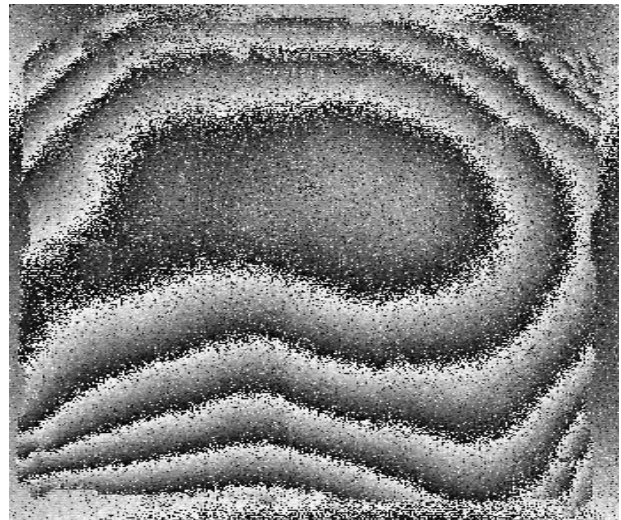


Figure 11. Wrapped full displacement map of the populated board fixed in the 4 corners, seen from the components side

**4.1.2 Results at a global level for the 5-point mounted assembly.**

The fringe pattern in Figure 12, recorded under thermal stress with the populated PCB mounted with all 5 screws, shows not only a different curvature of fringes on the PQFP component, but also discontinuities along some of its sides. One more experimental evidence: between the two states compared by the interferogram the PQFP pins have been elongated.



Figure 12. Wrapped, full displacement map of the populated board fixed in the 5 corners, seen from the components side

This observation opened the way towards a third series of measurements, localized near the sides (and the pins) of the integrated circuit.

**4.1.3 Results at a local level for the 5-point mounted assembly**

At this stage the interferograms are expected to provide quantitative values for the out-of-plane displacement in

particular regions of interest (near the sides of the component, for example). These data are necessary in order to provide solid explanations and proofs for possible physical origins of failure.

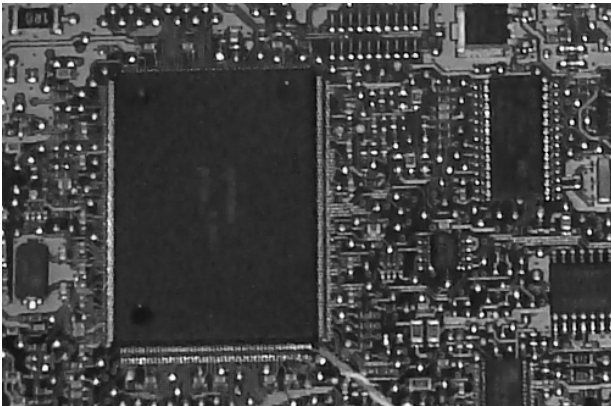


Figure 13. Region of interest chosen according to a high rate of destructive shear of solder joint

Temporal evolution of deformation: The results show the transient deformation of the PQFP component just after the heat stressing (Figure 14) as well as the more stable deformation after a few seconds (Figure 15).

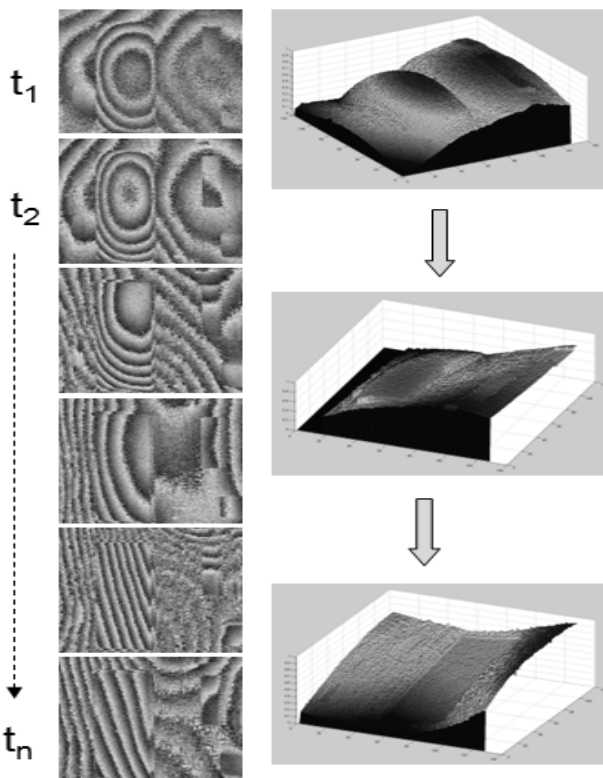


Figure 14. Transient thermal deformation

For another series of measurements, the final local deformation is shown in Figure 16.

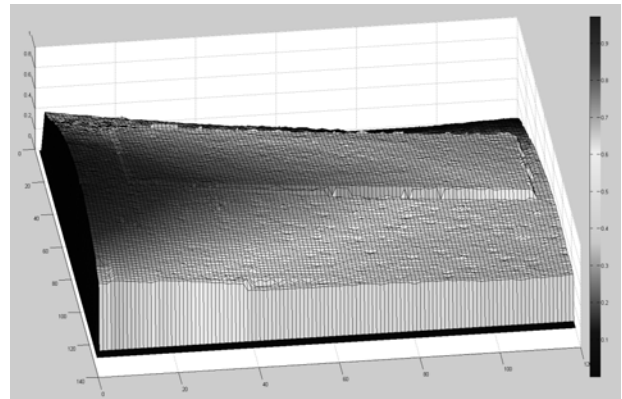


Figure 15. Final, stable thermal deformation

Tensile deformation of pins: This last situation allows detecting a very important detail: a non-uniform tensile deformation of the pins along a side of the PQFP. The tensile stress is leading to shear stress in the solder joints. This may also be seen in the closed-field interferogram presented in Figure 16.



Figure 16. Detailed interferogram showing the fringe pattern on and around the PQFP under thermal stress

The wrapped phase fringe pattern in Figure 16 was unwrapped and is presented in the lower part of Figure 17.

Since the pins are perpendicular on the plane of the interferographic image, they cannot be seen. Therefore their elongation was calculated as the difference between the out-of-plane displacements along the two closed vertical lines on the displacement map in the lower part of Figure 17, between the two horizontal lines delimiting the PQFP. The displacements along these two closed vertical lines are shown in the graph presented in the central part of Figure 17, and their difference (that is, the tensile pins elongation) is presented in the graph visible in the upper part of Figure 17. On the horizontal axis the unit is pixels, on the vertical one the unit is radians, see eq.(5).

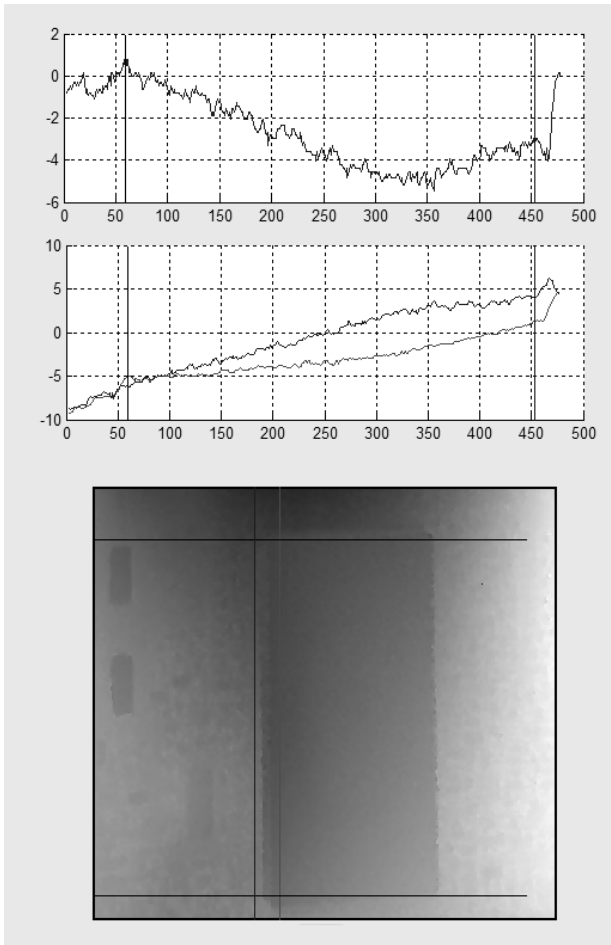


Figure 17. Unwrapped displacement map on and around the PQFP and calculation of tensile pins elongations

The conclusion of this result may be presented as in Figure 18.

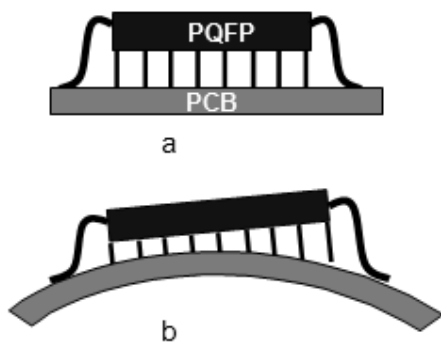


Figure 18. a - initial relative positions; b – final relative positions

One may remark that in case of only 4 screws for mounting the PCB, the curvature was more uniformly distributed across the PCB surface, and no discontinuity was noticed in the fringe pattern. That is true. It also means that this situation is produced by the curvature imposed by the central fastening screw, as proved by the result shown in Figure 18.

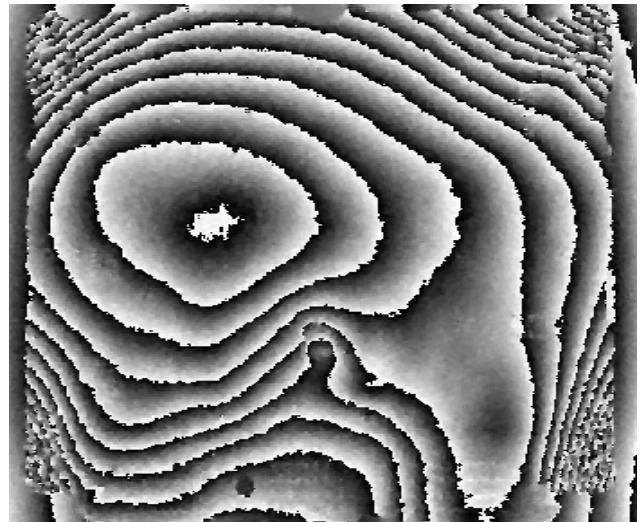


Figure 19. Wrapped phase fringe pattern of the PCBA seen from the side opposite to components

The interferogram in Figure 19 shows the same situation (5 screws, assembled PCBA) from the side opposite to components. The fifth screw is imposing a strong curvature to the PCB (see Figure 20) in the region where the large component is placed. Since it cannot follow this strong curvature, the PQFP exerts a flexure moment upon the PCB through the pins; the pins are thus under a strong tensile stress, able to produce solder joint failure by shearing.

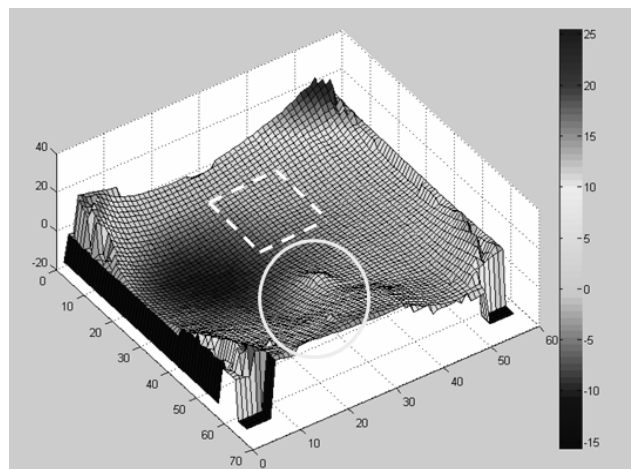


Figure 20. Explicit cartography of out-of-plane displacement field on the PCB side opposite to components

#### 4.2 Results for the electronic assembly under vibration stress

By examining the vibration amplitude maps the remarks on the effects of the fifth, central screw concerning the local state of strain and stress in the region near the PQFP component are similar in the case of assembly stressing by vibrations. Figure 21 presents the time-average interferogram obtained for one of the resonance frequencies of the electronic assembly, to be compared with the one presented in Figure 3.

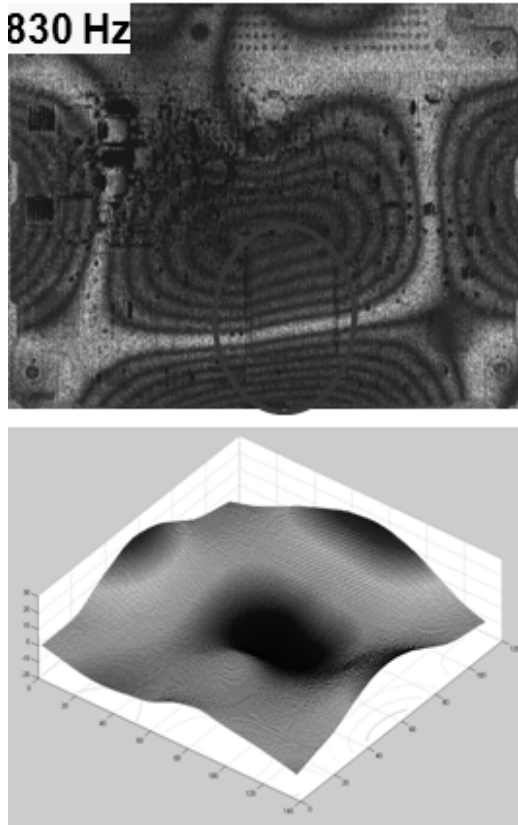


Figure 21 Left, eigenmode of the fully populated PCB; right, explicit vibration amplitude map

In Figure 22 we present a back to back comparison of several of the eigenmodes obtained for the two mounting configurations. As expected, along with a diminution of the vibration amplitudes we can see a slight augmentation of the corresponding resonance frequencies.

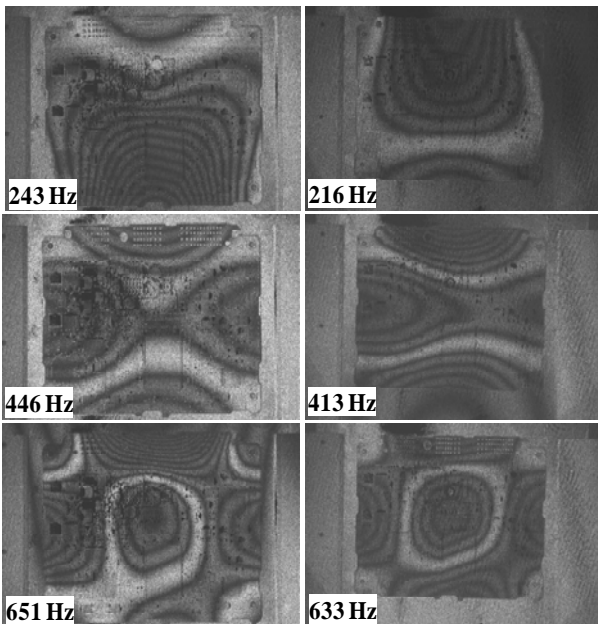


Figure 22. Several eigenmodes obtained for the 4 screw mounted (on the left) and 5 screw mounted electronic board

### 4.3. Local resonances

Local resonances of PQFP component: By using the real-time, time-average method some local resonances have been detected. These resonances may be very dangerous since the vibration amplitudes may become large and thus produce fatigue, finally leading to failure.

Some of the most important eigenmodes of the PQFP RISC component are shown by the interferograms presented in Figure 23.

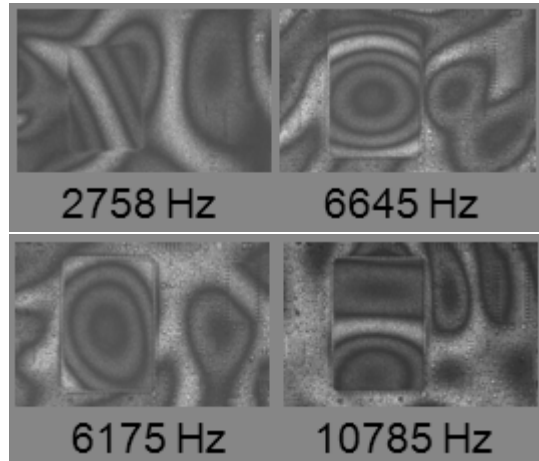


Figure 23. Four resonant modes of the RISC component

At an even lower scale, one may measure the eigenmodes of the PQFP pins (Figure 24). They are characterized by higher frequencies and by the fact that different pins resonate at different frequencies. Like in the previous case, the most important danger is fatigue.

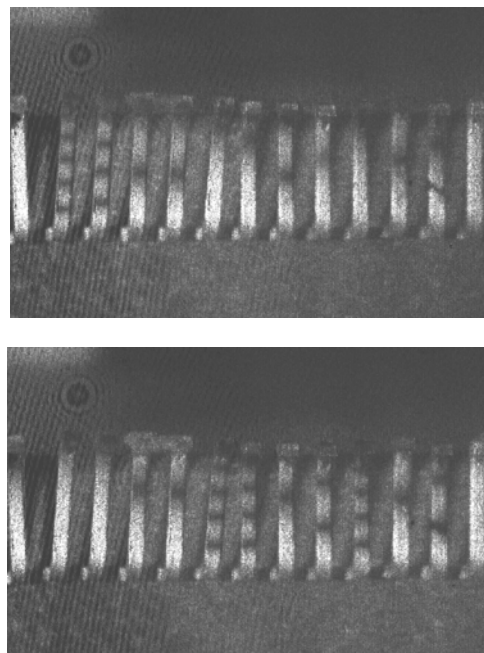


Figure 24. Pins eigenmodes at 13 338 Hz (upper image) and 13 628 Hz (lower image)

## 5. CONCLUSIONS

The use of out-of-plane laser speckle interferometry allows an experimental examination, at global level and local level, of the full deformation field of a PCBA subjected to thermal stress. The technique is non-contact and uses only very low thermal stress levels.

It is important to know that in this very complex field, testing of thermo-mechanical effects on embedded electronics, each experimental technique brings its own contribution and these contributions are complementary in discovering the failure mechanisms and their physical origins.

Further and ongoing research is aiming at the introduction of a high-rate camera and the adaptation of the present hardware and software so as to be able to study dynamic deformations.

The presented method was successfully applied to investigate the solder joint failure mechanism on certain sides of a large PQFP device on an embedded electronic board.

The results may also be useful in guiding work in numeric modelling towards phenomena able to conduct to failure of this kind of embedded electronic packaging. In fact, the negative contribution of the boundary conditions created by the fifth, central mounting screw to the mechanical stress localized in the solder joints is unfortunately in opposition with other mechanical conditions, like increasing the resonant frequencies of the assembly.

## 6. ACKNOWLEDGEMENTS

The authors acknowledge the creative collaboration and inspiring discussions with many specialists in related fields, in the frame of the AUDACE project of the MOV'EO Competitivity Pole.

A particular mention to the most closely involved persons, Mr. J.-Ph. Roux from CEVAA, Mr. A. El Hami from INSA and Mr. Ph. Pougnet from VALEO. The financial support of Direction Générale des Entreprises and of Conseil Régional de Haute-Normandie was essential for the Photomechanics Laboratory of INSA Rouen, where this work was conducted.

## 7. REFERENCES

- [1] Abdul J, Guo N, Du H, Wong BS and Chan KC. Non-destructive Evaluation of the Interface Between Silicon Dies and Copper Leadframes in Integrated Circuit Packaging. In: Proceedings of the International

Conference on Advanced Technology in Experimental Mechanics, Fukuoka, Japan, 2007

- [2] Borza DN. Mechanical vibration measurement by high-resolution time-averaged digital holography. *Measurement Science and Technology* 2005; 16, pp. 1853–1864.
- [3] Creath K. Phase-shifting speckle interferometry. *Applied Optics*, 24(18), O.S.A., 1985
- [4] Dantal B, Zimmerman MA, Saigal A. Characterization of a new Titanium dioxide-polymer composite material for electronic packaging applications. In: Proceedings of 13-th ICEM Conference, Alexandroupolis, Greece, 2007
- [5] Ding H, Powell RE, Hanna CR, Ume IC, Warpage measurement comparison using shadow Moiré and projection Moiré methods. In: Proceedings of 52nd electronic components and technology conference ECTC'02
- [6] Jacquot P, Slangen P, Borza D N. chapter 5, pp. 143-171, *Éléments d'interférométrie speckle*. In: Hermès – Lavoisier, editor. *Mesures de champs et identification en mécanique des solides, Traité MIM*, 2011
- [7] Jones R., Wykes, C., *Holographic and Speckle Interferometry*. Cambridge University Press, 1989
- [8] Lee B-W, Jang W, Kim D-W, Jeong J-H, Nah J-W, Paik K-W, Kwon D. Application of electronic speckle-pattern interferometry to measure in-plane thermal displacement in flip-chip packages. *Materials science & engineering A, Structural materials: properties, microstructure and processing*, 380 (Elsevier), 2004
- [9] Mukadam M, Meilunas M, Borgesen P, Srihari K. Assembly and reliability issues associated with leadless chip scale packages. In: *Int. Symposium on Microelectronics*, Boston MA, USA, 2003
- [10] Nistea I, Borza DN. Experimental analysis of failure in embedded electronics and mechatronical systems under thermal stress. *2010 IEEE-TTTC Proc. of Int. Conf. on Automation, Quality and Testing, Robotics, Cluj-Napoca, Romania*, 2010.
- [11] Shi X-Q, Pang H-L, Zhang X-R. Investigation of long-term reliability and failure mechanism of solder interconnections with multifunctional micro-moire interferometry system. *Microelectronics Reliability*, 44(5), Elsevier, 2004
- [12] Sutton MA, Ortu J-J, Schreier, HW. *Image Correlation for Shape, Motion and Deformation Measurements - Basic Concepts, Theory and Applications*. Springer, 2009

## 8. GLOSSARY

CCD: Charge-coupled device

INSA: Institut National des Sciences Appliquées de Rouen  
Nd-YAG: Neodmium-doped yttrium aluminum garnet

PCB: Printed circuit board

PCBA: Printed circuit board assembly

PQFP: Plastic quad flat pack

RISC: Reduced instruction set computer